Mechanism and Machine Theory 203 (2024) 105800

Contents lists available at ScienceDirect

Mechanism and Machine Theory

journal homepage: www.elsevier.com/locate/mechmt

Research paper

Simulation and validation of the transmission error, meshing stiffness, and load sharing of planetary spur gear transmissions

José I. Pedrero [a,*], Javier Sánchez-Espiga [b], Miryam B. Sánchez [a], Miguel Pleguezuelos [a], Alfonso Fernández-del-Rincón [b], Fernando Viadero [b]

[a] UNED, Departamento de Mecánica, Juan del Rosal 12, 28040 Madrid, Spain
[b] Universidad de Cantabria, Departamento de Ingeniería Estructural y Mecánica, Avda. de los Castros s/n, 39005 Santander, Spain

ARTICLE INFO

Keywords:
Planetary gears
Profile modification
Time-varying meshing stiffness
Load sharing
Transmission error

ABSTRACT

Although the load sharing between planets of sequentially phased planetary gear transmissions has been studied in the past, the required solving techniques based on the Finite Element Method result in long time consuming and high computational cost. This limits the possibilities of undertaking extensive studies that take into consideration a high number of cases allowing optimal solutions to be sought or general conclusions drawn. In addition, the determination of the curves of transmission error, time-varying mesh stiffness, and load sharing among tooth pairs in simultaneous contact are also complicated. In this work an analytical model has been developed for the simulation of the time-varying mesh stiffness, quasi-static transmission error, and load sharing ratio between planets and tooth pairs of planetary spur gear transmissions. It is based on similar models for external and internal spur gears previously developed and has been validated by comparison with a hybrid model based on the Finite Element Method and theoretic-experimental correlation.

1. Introduction

Planetary gearboxes are widely used in a variety of mechanical transmission systems, including those found in wind turbines, mining equipment, industrial machinery, and automobile vehicles. Using a planetary gear train has several advantages, including reduced vibration, compact size, light weight, high output torque, high speed reduction ratio, high transmission efficiency, and stable operation [1-4].

The planetary gear mechanism consists of several sets of cylindrical gear pairs with internal and external meshing. The investigation of a basic gear pair gives the basis for the study of a more complex planetary gear system. The geometry and design of internal and external gears are quite comparable. Similar constraints on teeth pointing, undercut, root interference, etc., should be regarded, as well as a specific secondary interference, also named tip interference, in the internal meshes, which may occur when there are a similar number of teeth on pinion and ring [5-6].

It is essential to accurately evaluate the mesh stiffness and transmission error when investigating into gear vibrations. The transmission error (TE), vibration, and noise characteristics of the planetary gear system are significantly influenced by its time-varying mesh stiffness (TVMS). In a gear transmission system, the TVMS is one of the main sources of vibration. Understanding the

* Corresponding author.
E-mail address: jpedrero@ind.uned.es (J.I. Pedrero).

https://doi.org/10.1016/j.mechmachtheory.2024.105800
Received 2 July 2024; Received in revised form 25 September 2024; Accepted 25 September 2024
Available online 5 October 2024

Nomenclature

Symbols

b	Face width, mm
E	Young's modulus, MPa
F	Load, N
F_T	Total load, N
h	Depth of the local FEM model, mm
K_M	Single mesh stiffness, N/mm
K^*_{Mmax}	Amplitude of single mesh stiffness per unit face width, N/mm^2
K_P	Mesh stiffness of the planet, N/mm
K_T	Time-varying meshing stiffness, N/mm
L	Half-length of the load distribution along the flank, mm
N_P	Number of planets
R	Load sharing ratio
r_b	Base radius, mm
r_C	Contact point radius, mm
Z	Number of teeth
$\Delta\xi_R$	Length of modification
Δ_R	Depth of modification at the tooth tip, μm
δ	Tooth pair deflection, transmission error, μm
δ_G	Separation distance, μm
δ_R	Depth of profile modification, μm
ε_α	Transverse contact ratio
υ	Poisson's ratio
ξ	Linear coordinate along the path of contact
T_{in}	Input torque, N·m

Subscripts

inn	Theoretical inner point of contact
ext	Extended contact model
max	Actual outer point of contact
min	Actual inner point of contact
out	Theoretical outer point of contact
PR	Planet-ring meshing
PS	Planet-sun meshing
P	Planet gear
R	Ring gear
S	Sun gear
1	Driving gear (pinion)
2	Driven gear (wheel / ring gear)

Abbreviations

LSR	Load sharing ratio
FE(M)	Finite element (models)
PPTE	Peak-to-peak amplitude of transmission error
QSTE	Quasi-static transmission error
SMS	Single mesh stiffness
TE	Transmission error
TVMS	Time-varying mesh stiffness
3D-LTCA	Loaded tooth contact analysis

dynamic properties of a planetary gear set requires an effective and efficient method to analyze the TVMS. The most widely used techniques for determining and analyzing mesh stiffness of cylindrical gear pair are analytical methods [4,7–19], finite element (FE) methods [1,20–26], and analytical-FE hybrid techniques.

The potential energy method [7,10, 17-19] is the most commonly employed analytical technique. It can be extended to three-dimensional spaces by using the slicing method [27,28]. The FE method takes time since it needs to simulate every gear pair that meshes in order to calculate the mesh stiffness of a variety of gear pairs and contact positions. On the contrary, an analytical method could provide an overall solution to the mesh stiffness calculation. Although the accuracy of FE methods is high, the efficiency is lower than that of analytical methods. To address this issue, some researchers [29] employed the adaptive local mesh refinement technique

in contact areas, which resulted in a precise and effective analysis of meshing features. In order to increase the effectiveness of the nonlinear FE contact methodology, other researchers [30] presented a point-to-surface contact analysis technique.

There is still a large efficiency difference between analytical and FE methods in spite of these advances. This gap is filled by the three-dimensional loaded tooth contact analysis (3D-LTCA), a representative analytical-FE method that combines the best features of both analytical and FE techniques. By doing away with the requirement for dense meshes and nonlinear contact algorithms, 3D-LTCA considerably improves computational efficiency when compared to FE methods. 3D-LTCA conveniently examines the problem of three-dimensional simulation without considering slice coupling effect into account, unlike analytical methods. Recent studies in this field related to planetary gears can be found in [31-34]. Nevertheless, requirements in processing time and computational cost of analytical-FE methods are noticeably stronger than analytical methods based on the potential energy method.

Numerous investigations have been conducted on transmission errors, meshing stiffness, and load distribution in planetary gears. Qin [35] proposed a dynamics modeling of faulty planetary gearboxes by TVMS excitation of spherical overlapping pittings and established a new TVMS model considering time-varying friction to characterize the spherical overlapping pittings, and a piecewise integration method was proposed for calculating multiple tooth meshing contact lines. Parker [36] investigated the vibration properties of planetary/epicyclic gears that arose from their cyclic symmetry, and derived results for spur and helical gear systems, two- and three-dimensional models, systems modeled with FE or analytically, systems with any combination of elastically deformable and rigid-body components, and systems with and without high-speed gyroscopic effects, without use of a specific mathematical model.

Tian et al. [37] presented a method for calculating TVMS by developing a stiffness model for elastohydrodynamic lubrication and integrating it into 3D-LTCA. In [38] a new efficient and accurate FE-analytical slice model for load distribution analysis and optimization of planetary gear transmission in wind turbine is proposed, which is explicitly formulated by the geometry slice model of external/internal gear contact, original FE-analytical slice model for local contact deformation, and efficient FE model for global structural deformation.

In [39] the authors proposed an analytical model that can clarify the dynamic behaviors of the modified gear pair affected by multiple manufacturing errors, specifically pitch deviation and geometric eccentricity. To fill this gap, a comprehensive analytical gear mesh model is proposed considering tooth profile modification, pitch deviation, and geometric eccentricity. The calculation formulas for the TVMS and load sharing ratio (LSR) are derived considering the iterative change of gear pair meshing parameters with phase under the influence of multiple manufacturing errors.

In previous works, Del Rincon et al. [40] described an advanced model for the analysis of contact forces and deformations in spur gear transmissions using FE and analytical methods to calculate the TVMS, loaded transmission error, and LSR. In [41], Fernández et al. incorporated tooth tip relief and manufacturing defects for various transmitted torques. In order to examine the impact of manufacturing errors on the quasi-static behavior of a 3-planet planetary gear transmission, Iglesias et al. [42] used a model that combines analytical solutions with finite element models for contact force analyses. In [43], Sánchez-Espiga et al. examined how the occurrence of several parameters, including mesh phasing and various faults like tooth thickness and pinhole position errors, affects the behavior of planetary transmissions regarding load sharing. In [44] Sanchez-Espiga et al. proposed a numerical approach to the problem of the calculation of the load sharing in planetary gear transmissions by measuring the strains in the root of the sun gear teeth.

Viadero et al. in [45] assessed the possibility of using the orbits described by the sun gear in order to analyze the load sharing ratio in planetary gear transmissions. Furthermore, the study was extended to observe the impact of the floatability and different tangential pinhole position errors in the load borne in a single contact between a pair of teeth in comparison to the load per planet. A novel quasi-static model of a two-stage compound planetary gear train with eccentricity error was published recently [46], and the orbit result of a healthy gear was used to confirm the accuracy of the established model. Moreover, the impact of the eccentricity error on the time-domain response under different error combinations was examined and discussed.

In previous works [47-49] Pedrero, Sánchez, et al. developed an analytical model for the calculation of the TVMS and LSR of external spur gears based on the principle of minimum energy. This method was later extended to internal gears [50-51] and applied to the determination of the critical contact and tooth-root stresses. From both models and the hypothesis of equal relative displacement of the driving and driven teeth for all the tooth pairs in simultaneous contact (which can also be obtained from the principle of minimum energy [52]) models for the loaded transmission error (quasi-static transmission error, QSTE) for external and internal spur gears were presented [52-54].

Concerning the planetary gears, a model of mesh stiffness for the complete planetary gear stage was developed [55] based on the combination of the models for external [52-53] and internal [54] gears. The distribution of the input torque between the planets and the load sharing between all the tooth pairs in contact (considering sun-planet and planet-ring tooth pairs of all the planets) were studied and the critical load conditions were calculated. In this paper, the extension of this model to simulate the QSTE of planetary gears and its relationship with the TVMS and the LSR between planets and teeth is presented.

Accordingly, the objectives of the present research can be summarized as follows:

1. Develop an analytical model, simple and efficient, for the simulation of the time-varying meshing stiffness, load sharing between planets and teeth, and loaded transmission error for planetary spur gears.
2. Validate the proposed model with a hybrid model based on the FE models (FEM) and analytical formulations [40,42].
3. Study the influence of the profile modification on the load sharing, mesh stiffness and transmission error.

2. Background: models for external and internal spur gears

The model for planetary gears presented in this paper is based on the models previously presented for external [52-53] and internal

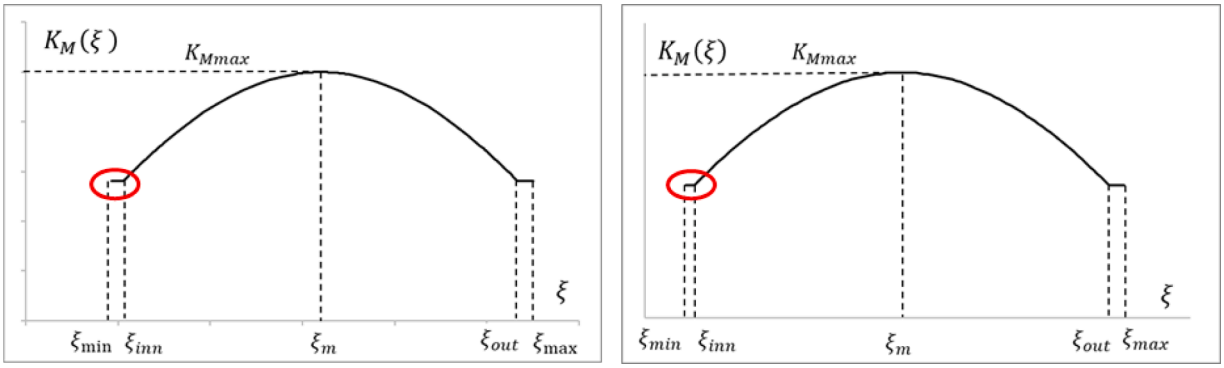

Fig. 1. Typical curves of single mesh stiffness of external (left) and internal (right) spur gears.

[54] spur gears. In this section, these previous models are briefly outlined to facilitate a better understanding of the more complex model presented herein. As these contains are not original, equations and diagrams have been reduced to strictly necessary. More detailed developments and explanations can be found in [47-55].

The formulation of the model of QSTE, $\delta(\xi)$, LSR, $R(\xi)$, and TVMS, $K_T(\xi)$, for both internal and external spur gears can be expressed as follows:

$$\delta(\xi) = \frac{F_T + \sum_j K_M(\xi + j)(\delta_G(\xi + j) + \delta_R(\xi + j))}{\sum_j K_M(\xi + j)} \tag{1}$$

$$R(\xi) = \frac{F(\xi)}{F_T} = \frac{K_M(\xi)}{F_T}(\delta(\xi) - (\delta_G(\xi) + \delta_R(\xi))) \tag{2}$$

$$K_T(\xi) = \frac{F_T}{\delta(\xi)} \tag{3}$$

in which $F(\xi)$ is the load at the tooth pair, F_T is the total load transmitted by the gear pair, $K_M(\xi)$ is the single mesh stiffness (SMS) which is the mesh stiffness of the tooth pair, $\delta_G(\xi)$ is the separation distance between driving and driven tooth profiles outside the theoretical contact interval (the separation distance is null inside), and $\delta_R(\xi)$ is the depth of profile modification. Sums in Eqn. (1) are extended to all the tooth pairs simultaneously in contact. ξ is a linear coordinate along the path of contact which describes the contact position of the tooth pair and is expressed as a function of the pinion tooth number Z_1, the radius of the pinion contact point r_{c1}, and the pinion base radius r_{b1} [47-53], as follows:

$$\xi = \frac{Z_1}{2\pi}\sqrt{\frac{r_{c1}^2}{r_{b1}^2} - 1} \tag{4}$$

The curve of SMS can be accurately approximated by the equation:

$$\begin{aligned} K_M(\xi) &= K^*_{Mmax} b \cos(b_0(\xi_{inn} - \xi_m)) \quad \text{for} \quad \xi_{\min} \le \xi \le \xi_{inn} \\ K_M(\xi) &= K^*_{Mmax} b \cos(b_0(\xi - \xi_m)) \quad \text{for} \quad \xi_{inn} \le \xi \le \xi_{out} \\ K_M(\xi) &= K^*_{Mmax} b \cos(b_0(\xi_{out} - \xi_m)) \quad \text{for} \quad \xi_{out} \le \xi \le \xi_{\max} \end{aligned} \tag{5}$$

which is valid both for external and internal spur gears, although the coefficients K^*_{Mmax}, b_0, and ξ_m should be calculated separately, as described in [47-49] for external gears and [50-51] for internal gears. In this equation, b is the face width, ξ_{inn} and ξ_{out} are the inner and outer limits of the theoretical contact interval, corresponding to the intersection points of the line of action with both addendum circumferences, and $\xi_{\min}$ and $\xi_{\max}$ are the inner and outer limits of the actual contact interval, which includes the additional contact intervals due to the loaded teeth deflections. $K_M(\xi)$ is uniform throughout the additional contact intervals because contact is not conjugate but occurs outside the pressure line, between the tip of one tooth and a very small interval of the mating tooth profile at the root, and therefore the variation of $K_M(\xi)$ is neglectable [52]. Fig. 1 presents the curve of single mesh stiffness for external and internal spur gears. It is observed that both curves are very similar, although the length of the additional contact intervals are almost identical for external gears, and quite different for internal gears, as highlighted in the figure. The symbol K_{Mmax} in the diagrams describes the local maximum of the SMS curve, but the specific value is not equal for external and internal gear. However, it should be pointed out that the ratio K_{Mmax} to $K_M\left(\xi_{min/max}\right)$ are the same in both cases, as shown in Fig. 1.

The separation distance is the distance in the pressure line corresponding to the rotation of the pinion tooth required to get contact with the wheel profile before reaching the theoretical inner point of contact, of after leaving the theoretical outer point of contact. The separation distance (also named approach distance) is null inside the theoretical contact interval and can be calculated from

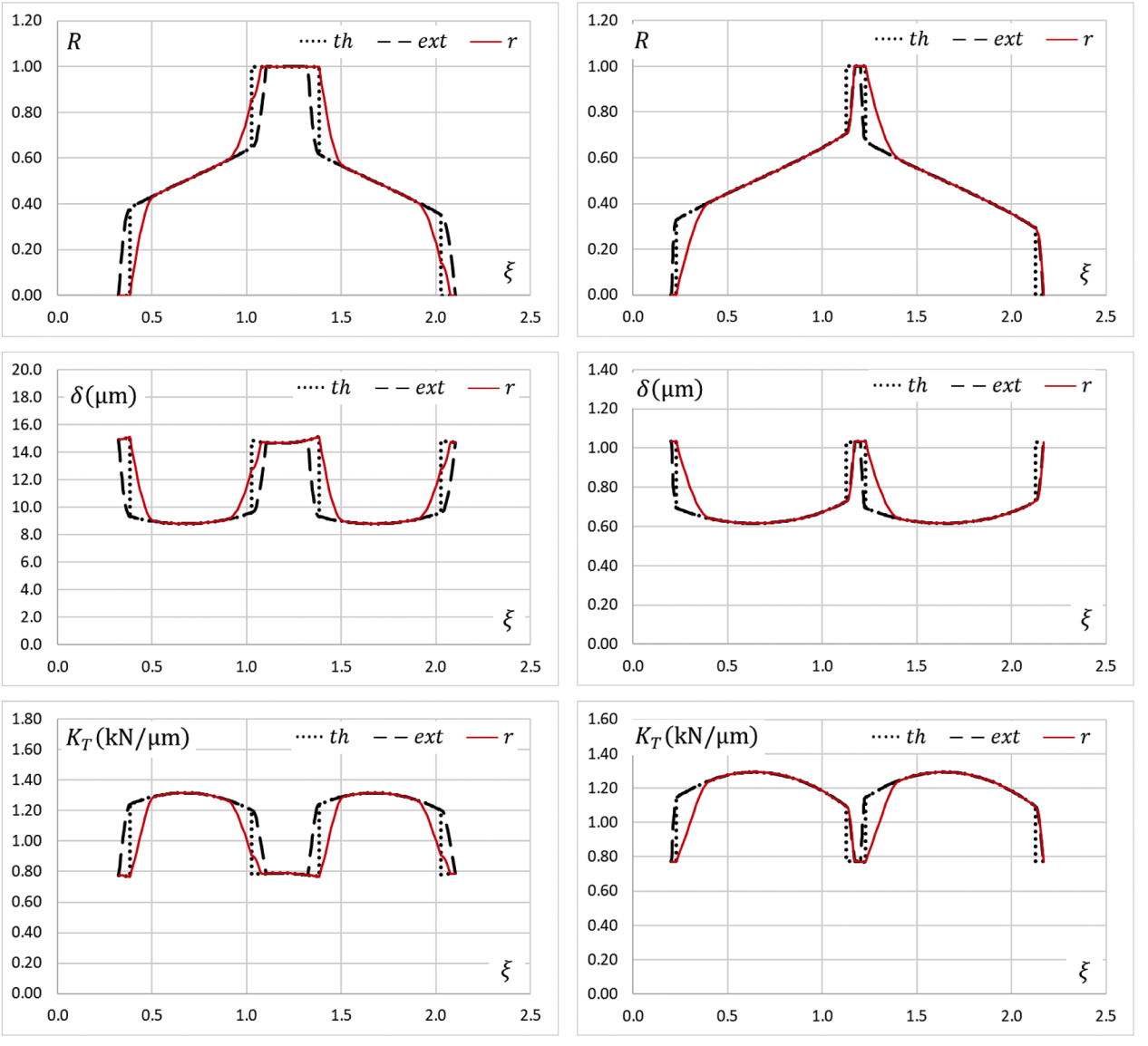

Fig. 2. LSR, QSTE, and TVMS for external spur gear with adjusted profile modification at the beginning of the contact and non-adjusted at the end of contact (left) and internal spur gear with adjusted profile modification at the beginning of the contact and no modification at the end of contact (right).

geometrical considerations. However, the resulting equation is complicated and can be accurately approximated by the following equation [52-54]:

$$\begin{aligned}
\delta_G(\xi) &= \left(\frac{2\pi}{Z_1}\right)^2 C_{p-inn}\, r_{b1}(\xi_{inn}-\xi)^2 \quad \text{for} \quad \xi_{\min} \le \xi \le \xi_{inn} \\
\delta_G(\xi) &= 0 \quad \text{for} \quad \xi_{inn} \le \xi \le \xi_{out} \\
\delta_G(\xi) &= \left(\frac{2\pi}{Z_1}\right)^2 C_{p-out}\, r_{b1}(\xi-\xi_{out})^2 \quad \text{for} \quad \xi_{out} \le \xi \le \xi_{\max}
\end{aligned} \tag{6}$$

The coefficients C_{p-inn} and C_{p-out} are different for external and internal gears. Their values can be computed as described in [52] and [54].

The profile modification is used to avoid the earlier start of contact produced by the teeth deflections, which induces the so-called mesh-in impact. The mesh-in impact is undesirable because it is a source of noise, vibrations, and dynamic load. The elimination of some amount of material at the tip of the driven teeth delays the start of contact, which can be moved to the theoretical point if the amount of eliminated material is suitable. In addition, the shape of modification allows to control the curve of QSTE. For linear or parabolic reliefs, the depth of modification is expressed as:

$$\begin{aligned}
\delta_R(\xi) &= \Delta_{R-inn} && \text{for} && \xi_{\min} \le \xi \le \xi_{inn} \\
\delta_R(\xi) &= \Delta_{R-inn}\left(1-\frac{\xi-\xi_{inn}}{\Delta\xi_{R-inn}}\right)^n && \text{for} && \xi_{inn} \le \xi \le \xi_{inn}+\Delta\xi_{R-inn} \\
\delta_R(\xi) &= 0 && \text{for} && \xi_{inn}+\Delta\xi_{R-inn} \le \xi \le \xi_{out}-\Delta\xi_{R-out} \\
\delta_R(\xi) &= \Delta_{R-out}\left(1-\frac{\xi_0-\xi}{\Delta\xi_{R-out}}\right)^n && \text{for} && \xi_{out}-\Delta\xi_{R-out} \le \xi \le \xi_{out} \\
\delta_R(\xi) &= \Delta_{R-out} && \text{for} && \xi_{out} \le \xi \le \xi_{\max}
\end{aligned} \tag{7}$$

where $\Delta\xi_R$ is the length of modification, Δ_R is the amount of modification, and the exponent n takes the values 1 and 2 for considering linear or parabolic reliefs, respectively. $\delta_R(\xi)$ is uniform outside the theoretical contact interval because, throughout the extended contact intervals, contact occurs between the tip of one tooth and the root of the mating tooth.

Finally, the limits of the effective contact interval, $\xi_{\min}$ and $\xi_{\max}$, can be calculated from the condition of null load, and therefore, according to Eqn. 2, by solving the equation:

$$\delta\left(\xi_{\min/\max}\right) = \delta_G\left(\xi_{\min/\max}\right) + \delta_R\left(\xi_{\min/\max}\right) \tag{8}$$

Fig. 2 show the curves of LSR, QSTE, and TVMS obtained from Eqns. (1) to (8). Solid lines in diagrams (*r* lines) correspond to an external spur gear with tip relief at both meshing teeth (which is called symmetric profile modification, left diagrams), and an internal spur gear with profile modification at the ring tooth tip only (asymmetric profile modification, right diagrams). In both cases, the amount of modification has been adjusted to shift the actual start of contact to the theorical inner point of contact. On the contrary, the amount of relief at the pinion tip of the external gear is not enough to avoid contact beyond the theoretical outer point of contact, and mesh-out push still occurs at the end of meshing. This can be appreciated in the LSR diagram by the parabolic unloading process at the upper limit of the contact interval. Dashed lines correspond to gears with no profile modification and can be obtained from the above equations by doing $\delta_R(\xi)=0$ (and therefore $\Delta_{R-inn}=\Delta_{R-out}=0$). The effective interval of contact $[\xi_{\min},\xi_{\max}]$ is in this case longer, for which it is called extended model (*ext*). Dotted lines correspond to the theoretical model (*th*), in which tooth deflections are neglected and is therefore suitable for very weakly loaded teeth. Theoretical curves can be obtained from the equations above by considering $\delta_G(\xi)=0$, except the limits of the contact interval, which are coincident with the theoretical ones and cannot be computed from Eqn. (8).

The above analytical model is suitable for non-standard teeth geometries or operating conditions, as non-standard center distance, non-standard tooth height -even different height on both meshing teeth-, undercut on pinion root, thinning for backlash allowance, or non-nominal load [53].

These models for external and internal gears can be combined to simulate planetary spur gears. In this case, there will be a lot of couple of teeth in simultaneous contact (up to four couples per planet, two at the planet-ring meshing and two at the planet-sun meshing), but the minimum elastic potential energy can be applied in the same way.

3. Model of meshing stiffness, load sharing and transmission error for planetary gears

The model of LSR, QSTE, and TVMS for planetary gears is based on the hypothesis of minimum elastic potential energy, as those for external and internal gears. From this hypothesis, the distance the meshing teeth approach each other can be demonstrated to be equal for all the tooth pairs in contact, including external and internal tooth pairs of all the planets. This relative distance is identified with the QSTE, and the TVMS is calculated as the ratio between the total load (which is equal to the torque at the planet carrier divided by the planet base radius) and the QSTE. The formulation is similar to the previous ones, but many tooth pairs in simultaneous contact should be considered (up to four times the number of planets), and a specific contact position for each one should be calculated.

In this section, the transmission error will be obtained and demonstrated to be equal for all the tooth pairs in simultaneous contact. Next, the corresponding contact points of the planet-ring meshing and the planet-sun meshing of each planet are calculated, and the corresponding meshing positions of the different planets are calculated as well. Finally, from these contact point parameters, the stiffness of each planet and the input torque distribution between planets are obtained.

The deformation δ^* of two meshing teeth which without load are separated a distance δ is given by:

$$\delta^* = \delta - (\delta_G + \delta_R) = \delta - \delta_{GR} \tag{9}$$

in which $(\delta_G + \delta_R)$ is denoted by δ_{GR} to simplify the notation. Accordingly, the load at a specific tooth pair is given by:

$$F_i = K_{Mi}(\delta_i - \delta_{GRi}) \tag{10}$$

The contribution of the tooth pair to the potential energy is:

$$U_i = \int_0^{\delta_i} F_i \mathrm{d}\delta = \int_{\delta_{GRi}}^{\delta_i} K_{Mi}\delta \mathrm{d}\delta = \frac{1}{2}K_{Mi}\left(\delta_i^2 - \delta_{GRi}^2\right) = \frac{1}{2}F_i(\delta_i + \delta_{GRi}) \tag{11}$$

and the total potential energy will therefore be:

$$U_T = \sum_i \frac{1}{2}F_i(\delta_i + \delta_{GRi}) = \sum_i \frac{1}{2}F_i\left(\frac{F_i}{K_{Mi}} + 2\delta_{GRi}\right) \tag{12}$$

The condition of minimum elastic potential energy can be obtained by means of the Lagrange's multipliers, as follows:

$$G = \sum_i \frac{1}{2}F_i\left(\frac{F_i}{K_{Mi}} + 2\delta_{GRi}\right) + \lambda\left(F_T - \sum_i F_i\right)$$

$$\frac{\partial G}{\partial F_i} = 0 \Rightarrow \frac{F_i}{K_{Mi}} + \delta_{GRi} - \lambda = 0 \Rightarrow F_i = K_{Mi}\lambda - K_{Mi}\delta_{GRi}$$

$$F_T = \lambda\sum_j K_{Mj} - \sum_j K_{Mj}\delta_{GRj} \Rightarrow \lambda = \frac{F_T + \sum_j K_{Mj}\delta_{GRj}}{\sum_j K_{Mj}} \tag{13}$$

resulting in:

$$F_i = K_{Mi}\left(\frac{F_T + \sum_j K_{Mj}\delta_{GRj}}{\sum_j K_{Mj}} - \delta_{GRi}\right) \tag{14}$$

Comparing Eqns. (10) and (14) it can be concluded that the distance the meshing teeth should approach each other is:

$$\delta_i = \frac{F_T + \sum_j K_{Mj}\delta_{GRj}}{\sum_j K_{Mj}} = \delta \tag{15}$$

which does not depend on i, and consequently is equal for all the tooth pairs in contact at this moment. δ describes the delay of the driven gear with respect to the driving gear and is therefore the QSTE. Finally, the TVMS is expressed as:

$$K_T = \frac{F_T}{\delta} \tag{16}$$

Eqs. (14) to (16) are very similar to Eqns. (1) to (3), and constitute the model of LSR, QSTE, and TVMS for planetary spur gears. The total load F_T is the equivalent load tangent to the planet base circumference, which induces a torque equal to that at the planet carrier T_{PC}:

$$F_T = \frac{T_{PC}}{r_{bP}} \tag{17}$$

where r_{bP} is the planet base radius. Sums in Eqns. (14) and (15) are extended to all the tooth pairs in contact at the specific contact position. Functions $K_M(\xi)$, $\delta_G(\xi)$, and $\delta_R(\xi)$ are all known, although expressions are different for external and internal teeth. The problem is to express the contact parameter ξ of all the tooth pairs as a function of that for one of them. If ξ_{PR} is the contact parameter of the reference pinion-ring tooth pair, it can be demonstrated that the corresponding parameter of the planet-sun tooth pair ξ_{PS} is given by [55]:

$$\xi_{PS} = \xi_{PR} - \left\{\frac{Z_P}{2}\left(1 - \frac{\alpha'_{t-PS} - \alpha'_{t-PR}}{\pi}\right)\right\} \tag{18}$$

where Z_P is the number of teeth of the planet, subscripts PS and PR denote the planet-sun and the planet-ring meshing, and $\{x\}$ function

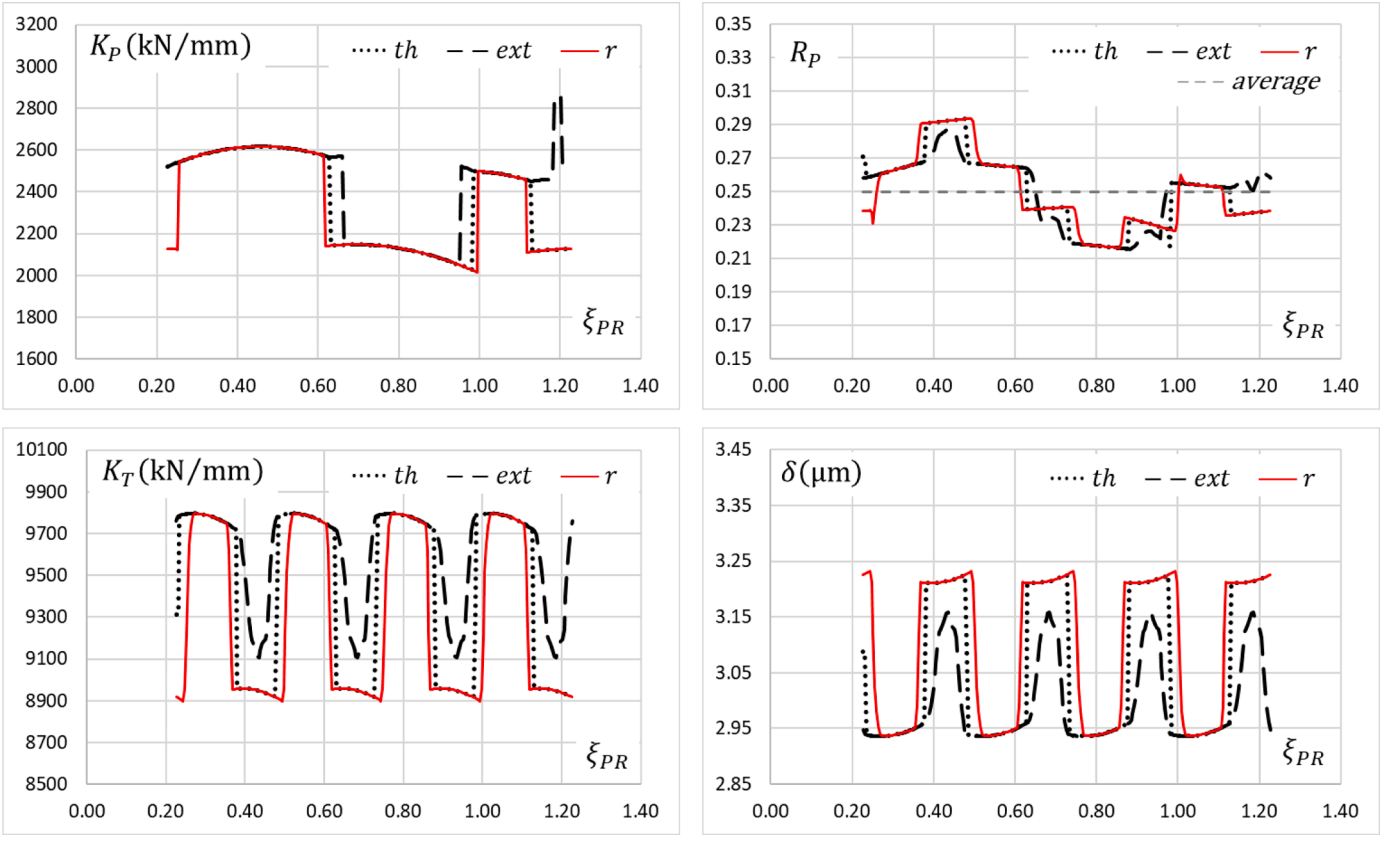

Fig. 3. Planet mesh stiffness (up-left), LSR between planets (up-right), TVMS (down-left), and QSTE (down-right) of four-planets planetary gear.

Table 1
Data of planetary stage.

	Sun	Planets	Ring
Module (mm)	4.00	4.00	4.00
Normal pressure angle (°)	20.00	20.00	20.00
Tooth addendum coefficient	1.00	1.00	1.00
Tooth dedendum coefficient	1.25	1.25	1.25
Tool tip radius coefficient	0.05	0.05	0.05
Number of teeth	37	23	83
Rack shift coefficient	0.00	−0.10	0.00
Outside radius (mm)	78.00	50.00	162.00
Operating center distance (mm)		120.00	
Face width (mm)	25.00	25.00	25.00
Input torque (N·m)	2000.00		
Number of planets		4	

denotes the fractional part of x. For sequentially phased planetary gear transmissions, the planet-ring contact parameter of the planet k can be expressed as a function of that of the reference planet, $k = 0$, as follows:

$$\xi_{PR}^{(k)} = \xi_{PR}^{(0)} + \frac{k}{N_P} \tag{19}$$

N_P being the number of planets. Of course, the tooth pairs in contact at a specific meshing position are all that verify:

$$\xi_{\min-PR/PS} \le \xi_{PR/PS}^{(k)} \le \xi_{\max-PR/PS} \tag{20}$$

Finaly, the mesh stiffness of the planets K_P can be calculated by:

$$K_P^{(k)}\left(\xi_{PR}^{(0)}\right) = \sum_i K_{M-PR}\left(\xi_{PR}^{(k)} + i\right) + \sum_j K_{M-PS}\left(\xi_{PS}^{(k)} + j\right) \tag{21}$$

and the LSR (or torque sharing ratio) between planets is expressed as:

$$R_P^{(k)}\left(\xi_{PR}^{(0)}\right) = \frac{K_P^{(k)}\left(\xi_{PR}^{(0)}\right)}{\sum_n K_P^{(n)}\left(\xi_{PR}^{(0)}\right)} \tag{22}$$

Fig. 3 shows the planet mesh stiffness, the LSR between planets, the TVMS of the planetary stage, and the QSTE of a planetary spur gear with four planets, described in Table 1, obtained from Eqns. (22), (16), and (15), respectively. Parabolic relief of 15 μm depth and 150 μm length has been applied to all the teeth of the planets, sun, and ring. The curves have been represented in the diagrams by solid lines (and denoted by *r*).

Curves corresponding to the theoretical model (*th*) and extended model (*ext*) have also been represented (dotted and dashed lines, respectively).

Fig. 4 shows the load at the planet-ring tooth-pairs, at the planet-sun ones, and at the most heavily loaded tooth-pair at any moment, all obtained from the combination of Eqns. (22) and (2). These curves can be applied to the assessment of bending and contact stresses and friction power losses.

4. Validation by hybrid approach

To validate the analytical formulation presented in Section 3, it is compared with the behavior obtained from the use of a hybrid model developed by some of the authors, presented in [40]. To explain this step in detail, it is necessary to set the focus on some of the specifics of this model. Thus, in Section 4.1 these details regarding the hybrid model are provided. In this case, the focus is set specially in the solution of the contact problem, which is the main difference between both approaches. Afterwards, in Section 4.2. the authors compare the results provided by using both different modelling approaches.

4.1. *Description of the hybrid model*

In this section, the authors provide the necessary details to understand the differences in both approaches to the modelling of planetary gear sets analyzed in this work. Firstly, this hybrid model combines analytical formulations and the use of FEM. As far as FEM are concerned, this model is based on the proposal presented by Vedmar and Henriksson [56]. This approach overcomes the problem of obtaining the meshing stiffness in the contact between active flanks by using the superposition principle to combine a series of FEM. More precisely, these models involve a global model, that represents a number of teeth Z and the body of the gear; and a local model, that only represents the geometry of the active flank up to a depth of h. Thus, by applying the same unitary load in the same point and opposite directions, the combination of the results of these two models provides the deformations supported by the gear, excluding the local distortion due to the use of point forces in the tooth flank. Those models are developed by using the Partial Differential Equation

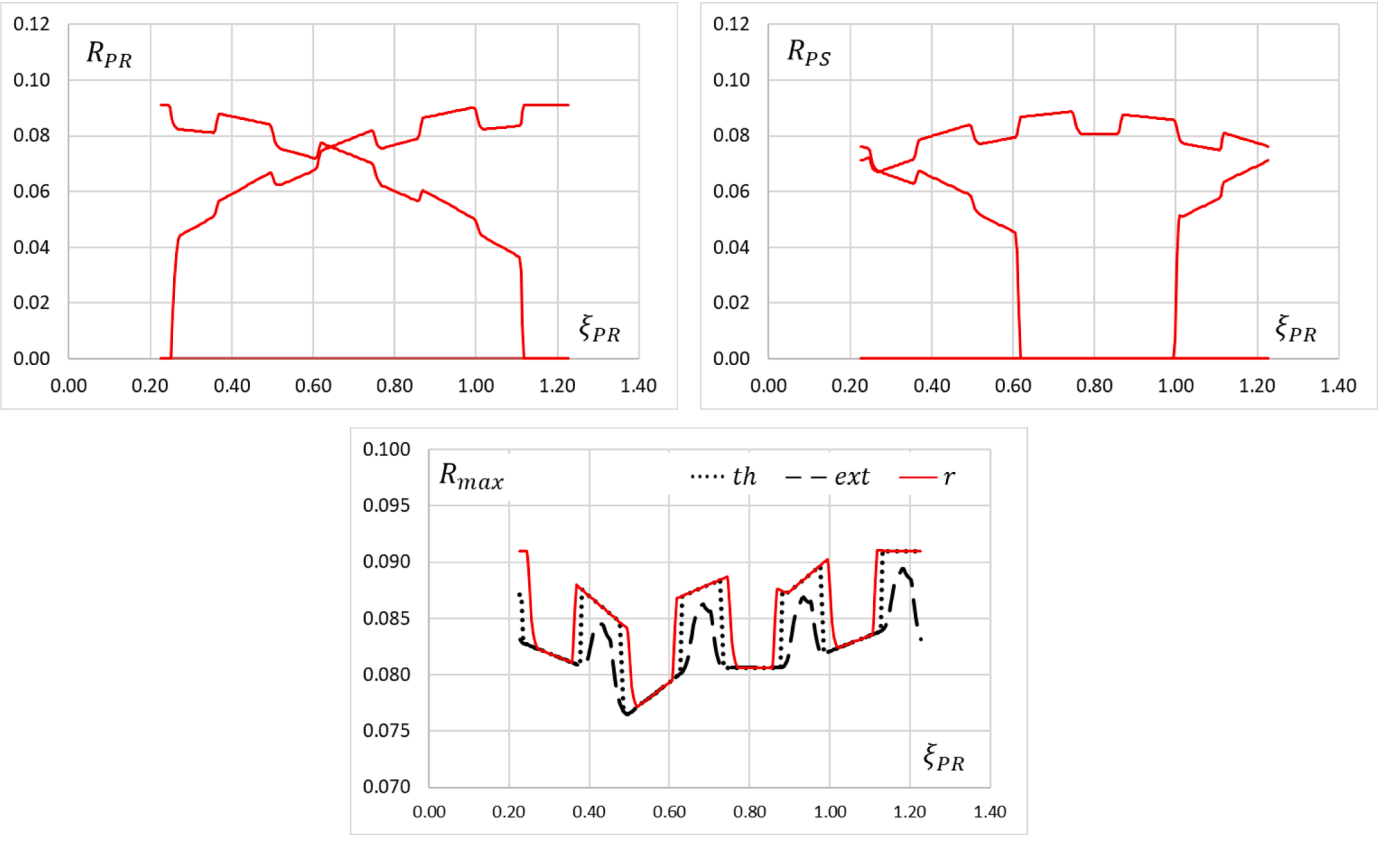

Fig. 4. Fraction of the total load at the planet-ring tooth pairs (up-left), at the planet-sun tooth pairs (up-right), and at the most heavily loaded tooth pair (down) of four-planets planetary gear.

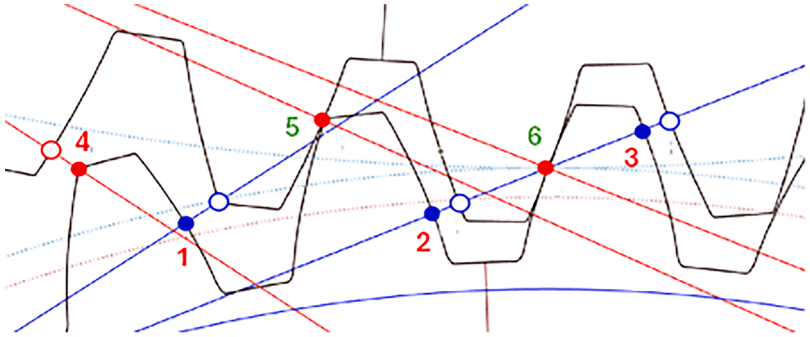

Fig. 5. Detail of the contacts consider for a given meshing position, positive overlaps (points 5–6) and negative overlaps (points 1–4).

Toolbox in MATLAB. These models are shaped using triangular elements with nodes in every vertex. Furthermore, in those models, the areas that belong to the interface between tooth flank and the rest of the tooth, in the local model, and the shaft mounting in the global one, are where the boundary conditions are applied. More precisely, these areas are modelled by considering them embedded.

For the calculation of the Z number of teeth, which involves the number of teeth affected by a given contact as seen in [40], the following equation is employed:

$$Z = 2 \cdot \text{ceil}(\varepsilon_\alpha + 1) \tag{23}$$

where ε_α corresponds to the contact ratio and ceil is the function that rounds this number to the next integer.

As a result of the mentioned process, the linear part of the contact between active flanks in gears is solved. However, the non-linear local contact is not solved yet. To this aim, the Weber-Banaschek formulation, presented in [40], is employed to solve the local contact between involute profiles of external gears. These formulations were also adapted and developed for internal gears in [40], more precisely, for the calculation of the length of the area along the flank in which the pressure is distributed. These formulas, gathered below, provide the deformation of a point at a h depth in relation to a point in the flank, for plane strain as in this case Eq. (24) is applied:

$$u_{local}(F) = \frac{2(1-\upsilon^2)}{\pi E}\frac{F}{b}\left[\ln\left(\frac{h}{L}+\sqrt{1+\left(\frac{h}{L}\right)^2}\right) - \frac{\upsilon}{1-\upsilon}\left(\frac{h}{L}\right)^2\left(\sqrt{1+\left(\frac{L}{h}\right)^2}-1\right)\right] \tag{24}$$

A relevant parameter in (24) is L that refers to the half of length of the pressure distribution along the flank, h refers to the depth of the point in which the deformations are calculated, E the Young's Modulus, and υ the Poisson's ratio.

Apart from all the calculations related to the solution of the meshing stiffness, in parallel this model solves the analytical problem to determine the distances between active flanks. The possible contact considered by the model are equal to Z, as shown in Fig. 5. This model calculates both the distances between direct and inverse flanks, giving the chance to consider the effect of the backlash. These distances provide the information to know which flanks are in contact. Thus, by considering that the flanks are infinitely rigid and allowing them to overlap, those pairs of teeth in which the overlap is positive are in contact. In those the algorithm explained above for contact solving is triggered. Moreover, in this calculation of the overlaps in successive steps the influence of the tip relief or other profile modification factors such as errors are included. These modify the overlaps, and even make some contact appear or disappear.

Once the meshing stiffness is determined and the overlaps between flanks too, there is a linear relationship between the stiffness obtained from the FEM and the overlaps, expressed in (25). Moreover, the effect of the non-linear local contact is added. By this combination the contact forces are extracted for each pair of teeth in contact.

$$\delta_j(\{\vec{r_P},\theta_P\},\{\vec{r_S},\ \theta_S\}) = u_{Tj}(\{\vec{r_P},\ \theta_P\},\ \{\vec{r_S},\ \theta_S\},\ \{F\}) \text{ for } F_i \geq 0;\ i,j = 1,\ldots,\ n \tag{25}$$

where δ_j is the overlap between profiles, $\{F\}$ is the unknown force vector, u_{Tj} are the elastic deflections, while r and θ represent the position with respect to the center of the wheel and its angular position, respectively, for the sun (S) or the planet (P) in this specific case. The procedure for planets and ring would be the same.

Once the contacts are located and the contact forces are determined, for a planetary transmission the balance must be established. This refers to the balance between input and output torque, Eq. (26), and the balance in each planet due to the contact with the sun and ring gears, respectively, Eq. (27). Once the iterative procedure employed to establish the balance in the transmission converges, not only the contact forces are known, but also are the angular position of all the elements and the deflections borne by every gear. With those data, the results are extracted.

$$\sum_{i=1}^{N} \overrightarrow{F_{i\ PS}} \times \overrightarrow{r_{bS}} = \overrightarrow{T_{in}} \tag{26}$$

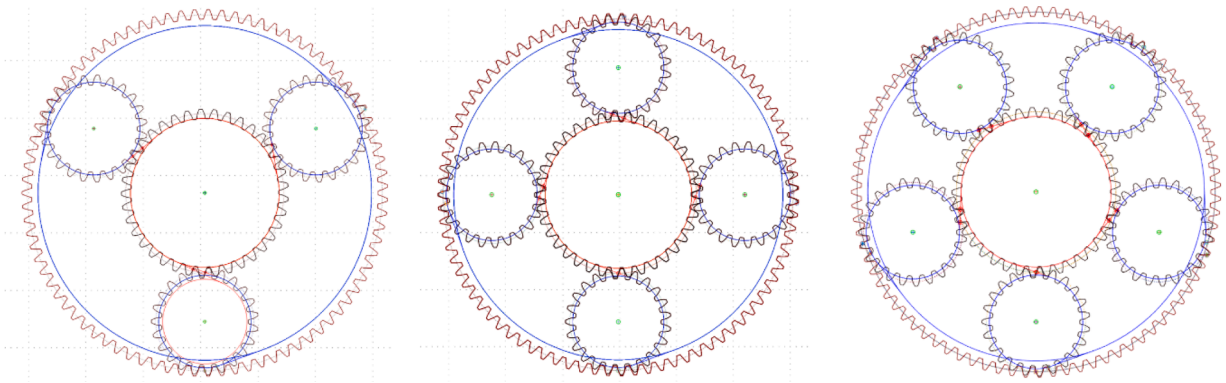

Fig. 6. Schematic representation of planetary gears considered in the validation study.

$$\overrightarrow{F_{i\,PS}} \times \overrightarrow{r_{bPi}} = \overrightarrow{F_{i\,Pr}} \times \overrightarrow{r_{bPi}} \tag{27}$$

where $\overrightarrow{F_{i\,PS}}$ corresponds with the contact force in the sun due to its contact with the i^{th}-planet or between planet and ring for (PR), $\overrightarrow{r_{bS}}$ is the base radius in either the sun (S) or the planet (P), and $\overrightarrow{T_{in}}$ is the input torque.

4.2. Comparison between analytic and hybrid models

Once the fundamentals of the models are clear, the next step, focus of this section, consists in the comparison of the results obtained from both approaches. In this specific case, the load distribution between planets, or more precisely the input torque distribution between planets, of three sequentially phased planetary gear transmissions have been studied from both analytic and hybrid models, described in Sections 2 and 3 and Section 4.1, respectively. A planetary gear as described in Table 1 but with 3, 4, and 5 planets has been considered. A schematic representation of three planetary gears is shown in Fig. 6.

To avoid edge contact, which may induce convergence problems in FE calculations, a small rounding has been applied to the teeth tip in the hybrid model; however, it has not been considered in the analytic model and the extended model has been used. The small rounding is equivalent to a profile modification with small depth and very small length, which has insignificant influence on the TVMS and consequently on the LSR. Even if the differences in the torque distribution between planets were not negligible, the trends of the curves will not be affected, so it should be sufficient to validate the model. Results can be seen in Fig. 7.

Although the numerical results of both models are not exactly the same, it is observed that the trends of the curves are very similar in all the cases, which ensures that analytic model is accurate enough for the simulation of planetary gears.

5. Influence of profile modification on TVMS and QSTE of planetary gears

The analytical model of TVMS and QSTE presented in Section 3 and validated in Section 4 can be applied to the analysis of the influence of profile modification on the dynamic behavior of the planetary gear. In fact, it is not easy to predict the influence of the relief geometry due to the large number of teeth in simultaneous contact and the continuously changing meshing conditions. Simulation using FEM-based techniques is time-consuming due to the relatively high computational cost and the large number of simulations required. However, the analytic method may provide approximate results with low computational cost and time consumption, and sufficient accuracy, at least for preliminary calculations. As an example, in this section the influence of the depth and length of the tip relief on the QSTE, planet mesh stiffness and LSR between planets will be analyzed.

5.1. Influence of the depth of modification

Tip relief should be deep enough to avoid mesh-in impact at the beginning of the contact. Clearly, the smaller the depth of relief the more similar the dynamic behavior of the modified teeth to that of unmodified teeth, including the existence of mesh-in impact, but too deep modifications result in smaller contact ratio and consequently greater loads at the teeth. The depth of modification is adjusted when the actual inner point of contact moves to its theoretical location. This occurs when the depth of modification is equal to the tooth-pair deflection (i.e., the QSTE) at the theoretical inner point of contact [52].

The adjusted depth of modification of the teeth of planetary gear presented in Table 1 is 3 μm for all the gears, sun, planets, and ring. This value is noticeably smaller than 15 μm considered in Fig. 3. Fig. 8 presents the curves of planet mesh stiffness, LSR between planets, TVMS of the planetary stage, and QSTE of the four-planets planetary spur gear described in Table 1, with adjusted depth of relief, $\Delta_{R-S} = \Delta_{R-P} = \Delta_{R-R} = 3$ μm. The length of modification remains equal to 150 μm.

It is observed that the curve of planet mesh stiffness with adjusted modification is almost identical to the theoretical one. The adjusted depth of modification in all the teeth moves the limits of the interval of contact to their theoretical locations, and the small

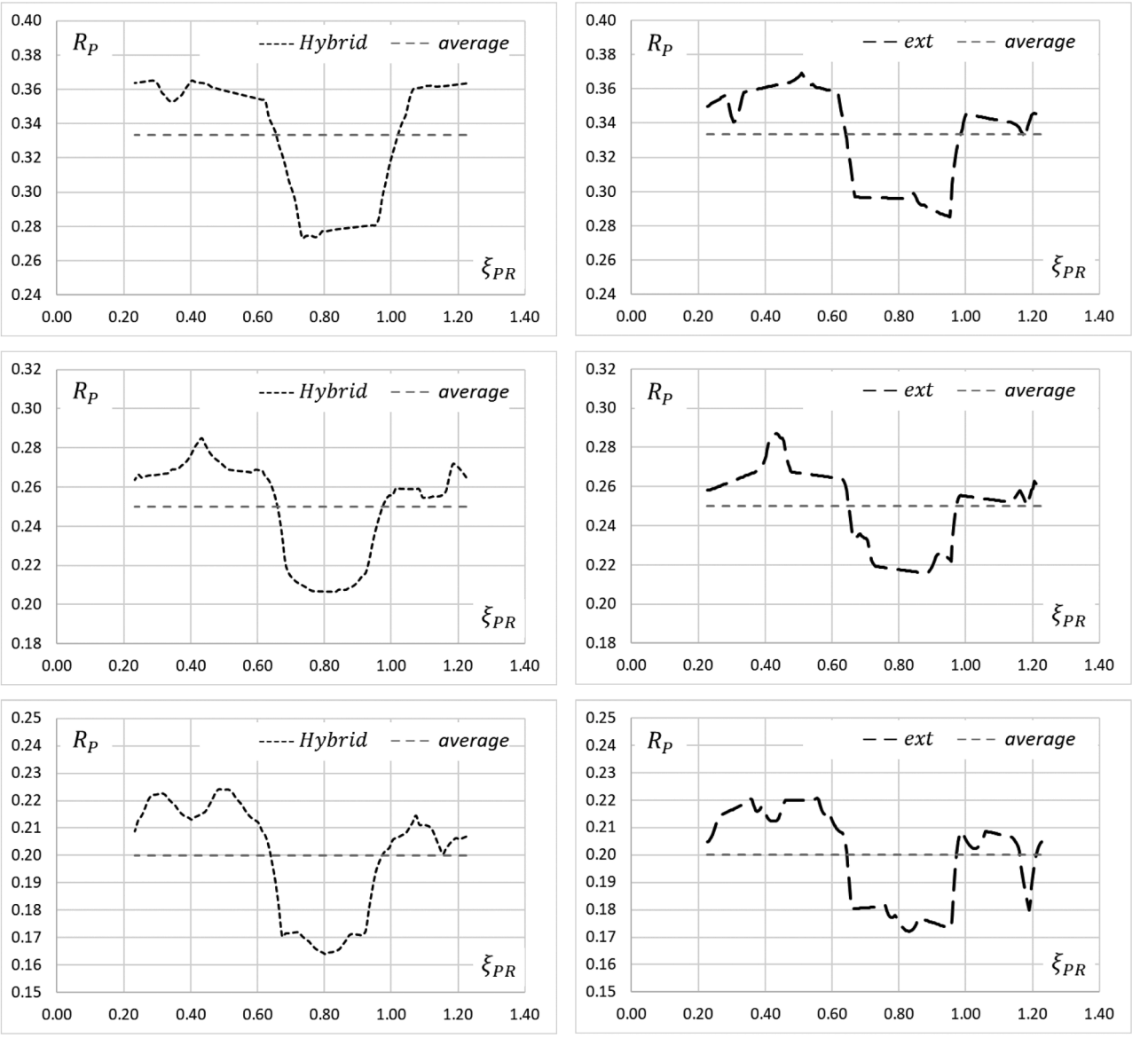

Fig. 7. LSR (torque distribution) between planets of planetary gear with three (up), four (middle), and five (down) planets, according to the hybrid model (left) and analytical model (right).

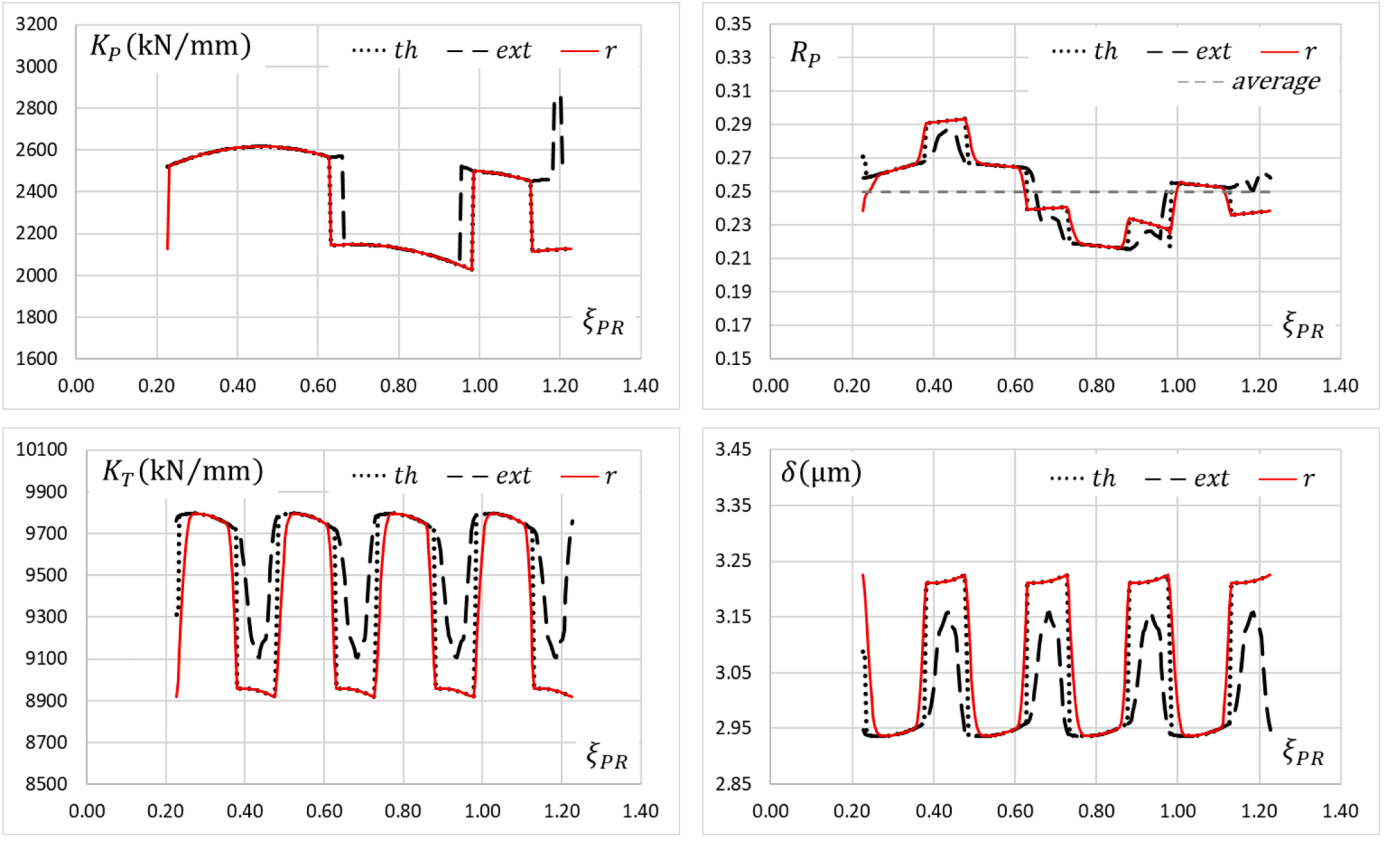

Fig. 8. Planet mesh stiffness (up-left), LSR between planets (up-right), TVMS (down-left), and QSTE (down-right) of four-planets planetary gear with adjusted depth of modification.

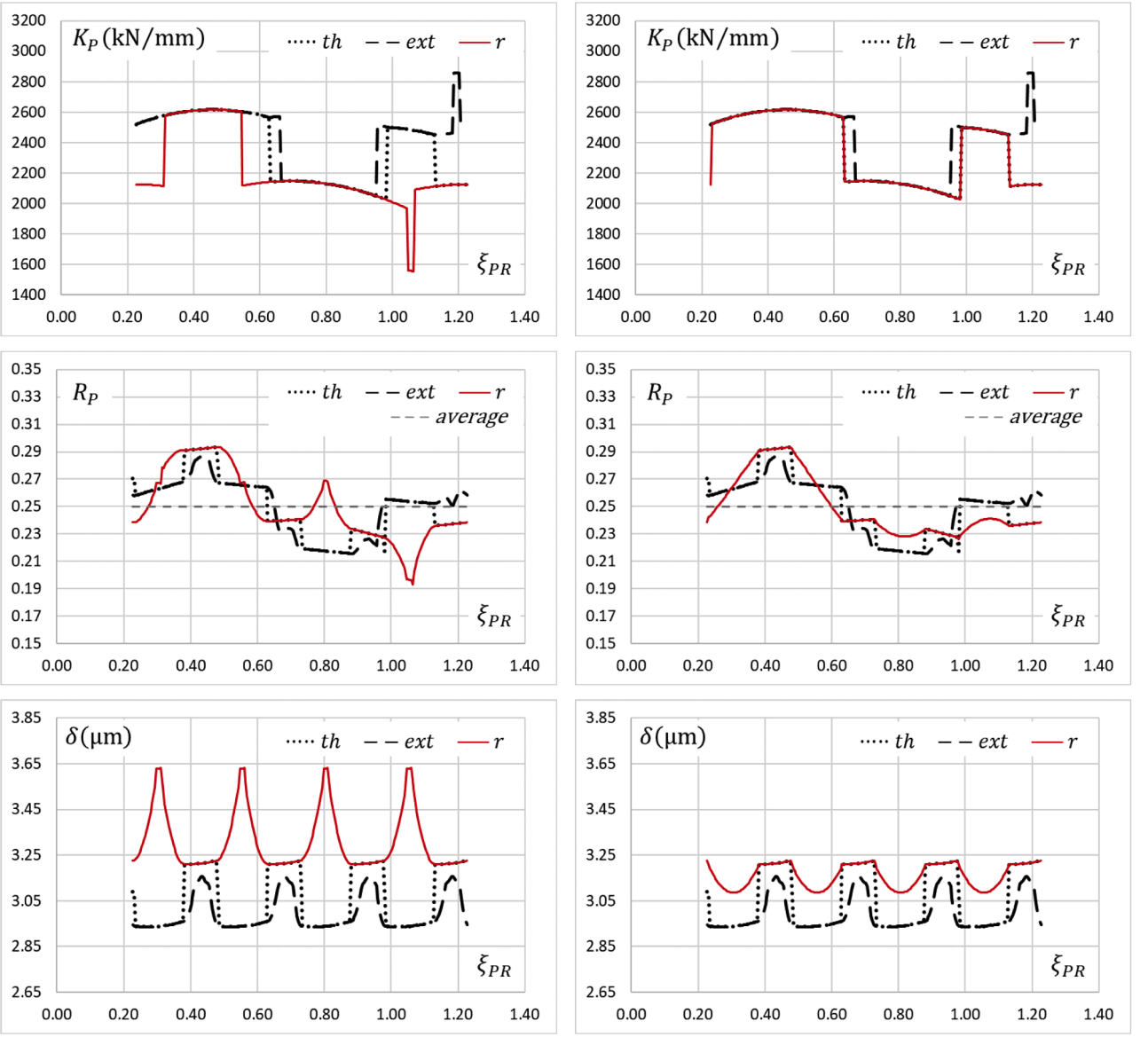

Fig. 9. Planet mesh stiffness (up), LSR between planets (middle), and QSTE (down) of four-planets planetary gear with deep (left) and adjusted (right) depth of modification.

length of modification influences very small sub-intervals along the contact interval, and therefore both curves are superimposed. This does not occur for non-adjusted depth of modification, as clearly observed in Fig. 3.

Similar effect can be observed in the curves of LSR between planets: the curve for adjusted depth of modification of Fig. 8 is much closer to the theoretical one than that for over relieved teeth of Fig. 3. However, differences between them are not great due once again to the small length of modification.

Similarly, the curves of TVMS and QSTE with adjusted depth of modification are closer to the theoretical ones than those for non-adjusted depth. Due to the small length of modification the differences between them are small, although the intervals of maximum TVMS and minimum QSTE (in which curves are coincident with theoretical and extended ones) are slightly wider for adjusted modification.

5.2. *Influence of the length of modification*

Longer modifications have stronger influence on the dynamic behavior of the planetary gear allowing to control important parameters as the load at the critical points or the peak-to-peak amplitude of transmission error (PPTE). The load at the critical points has obvious influence on the critical stresses and consequently on the load carrying capacity. The PPTE is related with the induced dynamic load (due to the variation of the output shaft velocity), noise, and vibrations.

The influence of the length of modification is quite different depending on the depth of modification. For a specific length of modification, the deeper the profile modification the stronger the influence on the dynamic behavior, because the depth of relief along the modification interval is greater. The length of modification considered in Figs. 3 and 8, namely 150 μm, is quite small. The interval of modification corresponds to a rotation of the planets of 0.006 rad and a value of the length of modification parameter $\Delta\xi_R = 0.022$.

Fig. 9 shows the curves of planet mesh stiffness, LSR between planets, and QSTE of the four-planets planetary spur gear considered above, with profile modification of $\Delta\xi_R = 0.15$ (corresponding to 900 μm length) and two different depths of modification, as considered in Figs. 3 and 8: 15 μm (left diagrams) and 3 μm (right diagrams, adjusted depth).

Diagrams of Fig. 9 present big differences with ones in Figs. 3 and 8, and between left and right diagrams of Fig. 9 as well. Below is a brief discussion on these results.

Regarding the planet mesh stiffness, for small length and/or depth of modification (Figs. 3, 8, and 9-right), the influence of the profile relief is very small, because contact conditions are identical along the entire contact interval except a very short portion (if small length), or except a longer portion but more similar conditions (if small depth). In addition, in each diagram the curves of the theoretical model (dotted line) and the model with profile modification (solid line) are almost identical because the influence of such a small modification on the effective contact ratio is quite insignificant. On the contrary, the curves of the extended modes (dashed lines), which do not consider profile modification, present some differences due to a stronger influence on the extended contact ratio. First, the intervals of maximum stiffness are wider, as corresponds to a greater contact ratio. Second, a peak arises around the point $\xi_{PR} = 1.2$. This is because the increase in the contact ratio induces a sooner start of contact and delayed end of contact of the tooth-pairs, and accordingly it is possible for a specific tooth pair to get contact before the end of contact of any other, resulting in one more tooth pair in simultaneous contact.

For greater length and depth of modification, the curve of planet mesh stiffness may be noticeably different. As seen in Fig. 9-left, the interval of maximum tooth pairs in simultaneous contact is clearly shorter than the previous ones due to the reduction in the effective contact ratio. In addition, around the point $\xi_{PR} = 1.05$ occurs just the opposite than before with the extended model: the smaller effective contact ratio results in one less tooth pair in contact, which induces a sudden reduction on the mesh stiffness. Consequently, along a small interval there are only two contacting tooth pairs, one of the planet-sun meshing and other of the planet-ring meshing.

Regarding LSR between planets, for small length of modification the curves corresponding to the theoretical and modified-profile models are quite similar, while the curve of the extended model is a little smoother but not very different from the previous two, as can be observed in Figs. 3 and 8. Specifically for adjusted depth of modification, the contact conditions are almost identical to the theoretical ones, and therefore corresponding LSR curves are almost identical too, as shown in Fig. 8. Extended curve is a little different due to the non-neglectable variation of the contact ratio.

Greater differences between three models are found for longer profile modifications, presented in Fig. 9. In this case, the curves of LSR between planets with profile modification are different from those of the other models, even for adjusted depth of modification. The contact conditions are different along the interval of modification, which influences the load sharing along a considerable part of the contact interval. For large length of modification and depth of modification, as in Fig. 9-left, the variation in the effective contact ratio may result in different number of teeth in simultaneous contact, and therefore the trend of the planets LSR curve is just the opposite to that of the theoretical and extended models along a long portion of the contact interval.

The greatest influence of the length of modification occurs on the QSTE. For small length of modification (Figs. 3 and 8) the curve of QSTE is almost identical to the theoretical one, and quite similar to the extended one, regardless of the depth of modification. However, for longer intervals of modification the curves of QSTE are entirely different, as shown in Fig. 9. It is observed that, for large depth of modification, the PPTE increases significantly. This is due to the reduction in the number of tooth pairs in contact, and subsequent reduction in the mesh stiffness. On the contrary, for adjusted depth of modification, the PPTE decreases significantly respect to that for small length of modification (Figs. 3 and 8) or no modification (extended model). This suggests the possibility to find an optimal length of modification for minimum PPTE.

Fig. 10 presents the curves of QSTE for the same four-planets planetary gear studied above, with adjusted depth of modification

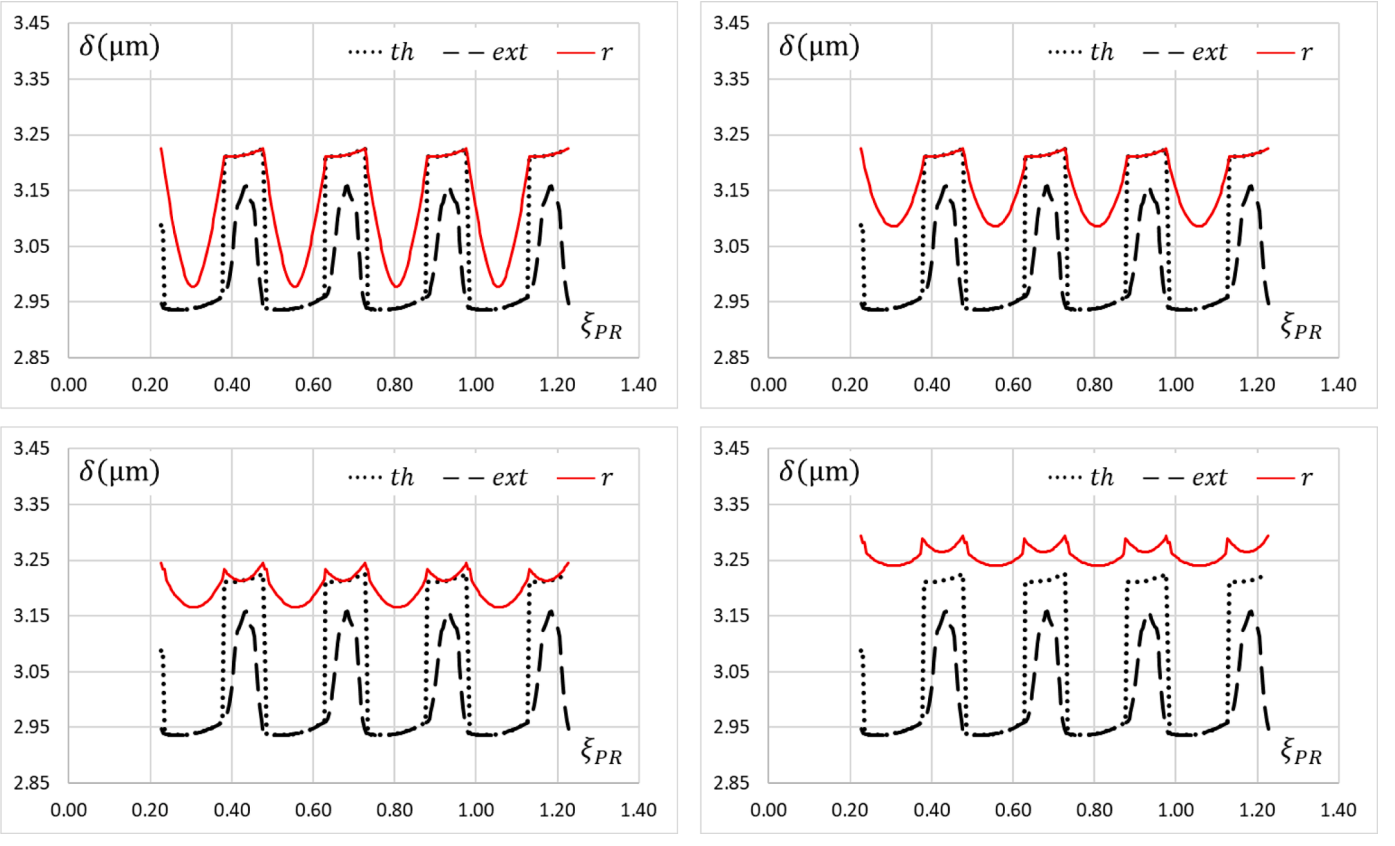

Fig. 10. QSTE of four-planets planetary gear with adjusted depth of modification, and length of modification 0.10 (up-left), 0.15 (up-right), 0.20 (down-left), and 0.27 (down-right).

$\Delta_{R-S} = \Delta_{R-P} = \Delta_{R-R} = 3$ μm, and four different lengths of modification $\Delta\xi_R$: 0.10, 0.15, 0.20, and 0.27.

It is observed that the QSTE increases as the length of modification increases. This result is obvious because the longer the interval of modification the smaller the mesh stiffness, and therefore the greater the QSTE. Nevertheless, the PPTE, which is the critical parameter to control the induced dynamic load and vibration, decreases. From Fig. 8, for small length of modification the PPTE is equal to the theoretical one, and the maximum and minimum values are equal in both cases. This theoretical PPTE for the considered four-planets planetary gear is 0.29 μm. As seen in the upper diagrams of Fig. 10, as the length of modification increases, the minimum QSTE increases, but the maximum remains unchanged, resulting in lower PPTE. For $\Delta\xi_R = 0.10$ (upper-left diagram) the PPTE is 0.25 μm; for $\Delta\xi_R = 0.15$ (upper-right diagram) the PPTE is 0.14 μm. If the length of modification continues to increase, the minimum QSTE continues to increase as well, but the maximum QSTE begins to increase slightly, as shown in the lower-left diagram of Fig. 10. Depending on the increases of the maximum and the minimum, the PPTE increases or decreases. If there is at least one point of the interval of maximum theoretical QSTE in which both curves, theoretical and modified profile QSTE, are tangent, it can be proved that the PPTE decreases. Lower-left diagram of Fig. 10 shows the curves of QSTE for a length of modification $\Delta\xi_R = 0.20$, for which the PPTE is 0.08 μm. If the length of modification continues to increase, there comes a time when the maximum QSTE grows more quickly than the minimum, so the PPTE begins to increase. For the considered planetary gear, the minimum PPTE is obtained for a length of modification $\Delta\xi_R = 0.27$, for which the PPTE is 0.05 μm, around 80% smaller than that with small (or without) modification.

6. Conclusions

An analytical model, simple and efficient, for the simulation of the time-varying meshing stiffness, load sharing, and quasi-static transmission error for planetary spur gears, which considers the influence of profile modification, has been developed. The uneven distribution of the torque between planets of sequentially phased planetary gears has been also studied. It is based on the application of the hypothesis of minimum potential energy to the simulation of the quasi-static transmission error, which has been demonstrated to be equal for all the tooth pairs in simultaneous contact, and its relationship with the time varying meshing stiffness and the load sharing ratio.

The model has been validated by comparison with a hybrid model based on finite element models and analytical formulation. The torque distribution between planets of three planetary gear sets with three, four, and five planets, respectively, has been considered, and very good fit between curves has been obtained in all the cases.

With the analytical model, the influence of the depth and length of profile modification has been analyzed. The following conclusions can be drawn:

1. For large depth of modification, for which contact does not occur at the outside points of the teeth profiles, the length of modification has small influence on the time-varying mesh stiffness, load sharing ratio and quasi-static transmission error.
2. For small depth of modification, for which contact occurs at the outside points of the profiles, the length of modification has strong influence on the time-varying mesh stiffness, load sharing ratio and quasi-static transmission error.
3. For adjusted depth of modification, for which the actual inner point of contact coincides with the theoretical one, the length of relief has strong influence on the peak-to-peak amplitude of transmission error, and an optimal length to minimize the amplitude, and consequently the induced dynamic loads, noise, and vibrations, can be found.

The analytical model requires much lower processing time and computational cost than other existing models based on the finite element method or similar computational techniques. This allows the influence of the gear parameters, geometrical and operational, on the behavior of the planetary gear to be studied almost instantaneously, even considering wide ranges, with not usual values, of these gear parameters, which allows the analysis to be extended to unexplored domains, with very low cost.

CRediT authorship contribution statement

José I. Pedrero: Writing – review & editing, Writing – original draft, Supervision, Methodology, Funding acquisition, Conceptualization. **Javier Sánchez-Espiga:** Writing – review & editing, Validation, Investigation. **Miryam B. Sánchez:** Writing – review & editing, Software, Investigation. **Miguel Pleguezuelos:** Writing – review & editing, Writing – original draft, Investigation. **Alfonso Fernández-del-Rincón:** Writing – review & editing, Writing – original draft, Validation, Supervision, Funding acquisition. **Fernando Viadero:** Writing – review & editing, Validation, Supervision.

Declaration of competing interest

The authors declare that they have no known competing financial interests or personal relationships that could have appeared to influence the work reported in this paper.

Data availability

No data was used for the research described in the article.

Acknowledgements

Thanks are expressed to the Spanish Council for Scientific and Technological Research for the support of the projects PID2022–142632OB-I00 "Model for the simulation of the load sharing and transmission error of planetary gears", PID2020–116213RB-I00 "Study of configuration and gear meshing phase on the dynamics of planetary transmissions: modelling and testing", and PID2023–147249OB-I00 "Development of enhanced methodologies for the evaluation of the load sharing impact on the planetary transmissions dynamics".

References

[1] A. Kahraman, Load sharing characteristics of planetary transmissions, Mech. Mach. Theory 29 (1994) 1151–1165.
[2] F. Chaari, T. Fakhfakh, M. Haddar, Dynamic analysis of a planetary gear failure caused by tooth pitting and cracking, J. Fail. Anal. Prev. 6 (2006) 73–78.
[3] A. Singh, Load sharing behavior in epicyclic gears: physical explanation and generalized formulation, Mech. Mach. Theory 45 (2010) 511–530.
[4] X.H. Liang, M.J. Zuo, T.H. Patel, Evaluating time-varying mesh stiffness of a planetary gear set using potential energy method, J. Mech. Eng. Sci. 228 (2014) 535–547.
[5] J.W. Polder, Interference and other limiting conditions of internal gears, ASME Design and Production Engineering Technical Conference, Paper 84-DET-180, Cambridge, MA (1984).
[6] F.L. Litvin, A. Fuentes, Gear Geometry and Applied Theory, 2nd ed., Cambridge University Press, Cambridge, 2004.
[7] D.C.H. Yang, J.Y. Lin, Hertzian damping, tooth friction and bending elasticity in gear impact dynamics, J. Mech. Des. 109 (1987) 189–196.
[8] P. Velex, M. Maatar, A mathematical model for analyzing the influence of shape deviations and mounting errors on gear dynamic behavior, J. Sound Vib. 191 (1996) 629–660.
[9] A. Kahraman, S. Vijayakar, Effect of internal gear flexibility on the quasi-static behavior of a planetary gear set, J. Mech. Des. 123 (2001) 408–415.
[10] P. Sainsot, P. Velex, O. Duverger, Contribution of gear body to tooth deflections-a new bidimensional analytical formula, J. Mech. Des. 126 (2004) 748–752.
[11] A. Bodas, A. Kahraman, Influence of carrier and gear manufacturing errors on the static load sharing behavior of planetary gear sets, JSME Int. J., Series C 47 (2004) 908–915.
[12] R.G. Parker, J. Lin, Mesh phasing relationships in planetary and epicyclic gears, J. Mech. Des. 126 (2004) 365–370.
[13] A. Singh, Application of a system level model to study the planetary load sharing behavior, J. Mech. Des. 127 (2005) 469–476.
[14] V. Abousleiman, P. Velex, A hybrid 3D finite element/lumped parameter model for quasi-static and dynamic analyses of planetary/epicyclic gear sets, Mech. Mach. Theory 41 (2006) 725–748.
[15] S. Wu, M.J. Zuo, A. Parey, Simulation of spur gear dynamics and estimation of fault growth, J. Sound Vib. 317 (2008) 608–624.
[16] H. Ligata, A. Kahraman, A. Singh, An experimental study of the influence of manufacturing errors on the planetary gear stresses and planet load sharing, J. Mech. Des. 130 (2008) 041701.
[17] Z. Chen, Y. Shao, Mesh stiffness calculation of a spur gear pair with tooth profile modification and tooth root crack, Mech. Mach. Theory 62 (2013) 63–74.
[18] L. Yang, L. Wang, Y. Shao, et al., A new calculation method for tooth fillet foundation stiffness of cracked spur gears, Eng. Fail. Anal. 121 (2021) 105173.
[19] Y. Han, X. Chen, J. Xiao, et al., An improved coupled-dynamic modeling for exploring gearbox vibrations considering local defects, J. Dyn. Monit. Diagnost. 2 (2023) 262–274.
[20] D.L. Seager, Load sharing among planet gears, SAE Transactions 79 (1970) 651–656. Paper No. 700178.
[21] T. Hidaka, Y. Terauchi, Dynamic behavior of planetary gear –1st Report: load distribution in planetary gear, Bull. JSME 19 (1976) 690–698.
[22] R.W. Cornell, Compliance and stress sensitivity of spur gear teeth, J. Mech. Des. 103 (1981) 447–459.
[23] P. Ma, M. Botman, Load sharing in a planetary gear stage in the presence of gear errors and misalignments, J. Mech., Transm., Autom. Des. 107 (1985) 4–10.
[24] T. Hayashi, Y. Li, I. Hayashi, et al., Measurement and some discussions on dynamic load sharing in planetary gears, Bull. JSME 29 (1986) 2290–2297.
[25] J. Wang, I. Howard, Finite element analysis of high contact ratio spur gears in mesh, J. Tribol. 127 (2005) 469–483.
[26] V.K. Tamminana, A. Kahraman, S. Vijayakar, A study of the relationship between the dynamic factors and the dynamic transmission error of spur gear pairs, J. Mech. Des. 129 (2007) 75–84.
[27] J.D. Smith, Estimation of the static load distribution factor for helical gears, J. Mech. Eng. Sci. 209 (1995) 193–199.
[28] J.J. Zhang, I.I. Esat, Y.H. Shi, Load analysis with varying mesh stiffness, Comput. Struct. 70 (1999) 273–280.
[29] M. Barbieri, A. Zippo, F. Pellicano, Adaptive grid-size finite element modeling of helical gear pairs, Mech. Mach. Theory 82 (2014) 17–32.
[30] C. Zhang, H. Dong, C. Zhang, et al., A node-to-surface linear complementarity problem approach for general three-dimensional contact analysis, Meccanica 56 (2021) 3079–3096.
[31] L. Chang, G. Liu, L.Y. Wu, A robust model for determining the mesh stiffness of cylindrical gears, Mech. Mach. Theory 87 (2015) 93–114.
[32] Y. Huangfu, X. Dong, K. Chen, et al., A tribo-dynamic based pitting evolution model of planetary gear sets: a topographical updating approach, Int. J. Mech. Sci. 220 (2022) 107157.
[33] P. Wang, H. Xu, H. Ma, et al., Effects of three types of bearing misalignments on dynamic characteristics of planetary gear set-rotor system, Mech. Syst. Sig. Process. 169 (2022) 108736.
[34] Z. Liu, C. Chang, H. Hu, et al., Dynamic characteristics of spur gear system with tooth root crack considering gearbox flexibility, Mech. Syst. Sig. Process. 208 (2024) 110966.
[35] Y. Qin, Q. Li, S. Wang, et al., Dynamics modeling of faulty planetary gearboxes by time-varying mesh stiffness excitation of spherical overlapping pittings, Mech. Syst. Sig. Process. 210 (2024) 111162.
[36] C. Wang, R.G. Parker, Symmetry-driven vibration behaviors in epicyclic/planetary gears: criticality of the mesh phase parameter, Mech. Syst. Sig. Process. 206 (2024) 110878.
[37] H. Tian, X. Zhao, W. Huang, et al., A stiffness model for EHL contact on smooth/rough surfaces and its application in mesh stiffness calculation of the planetary gear set, Tribol. Int. 196 (2024) 109720.
[38] C. Zhang, Y. Hu, Z. Hu, et al., FE-analytical slice model and verification test for load distribution analysis and optimization of planetary gear train in wind turbine, Eng. Fail. Anal. 162 (2024) 108451.
[39] L. Duan, L. Wang, W. Du, et al., Analytical method for time-varying meshing stiffness and dynamic responses of modified spur gears considering pitch deviation and geometric eccentricity, Mech. Syst. Sig. Process. 218 (2024) 111590.
[40] A.F. Del Rincón, F. Viadero, M. Iglesias, et al., A model for the study of meshing stiffness in spur gear transmissions, Mech. Mach. Theory 61 (2013) 30–58.
[41] A. Fernández del Rincón, M. Iglesias, A. de-Juan, et al., Gear transmission dynamic: effects of tooth profile deviations and support flexibility, Appl. Acoust. 77 (2014) 138–149.
[42] M. Iglesias, A. Fernández del Rincón, A. de-Juan, et al., Planetary transmission load sharing: manufacturing errors and system configuration study, Mech. Mach. Theory 111 (2017) 21–38.
[43] J. Sánchez-Espiga, A. Fernandez del Rincon, M. Iglesias, F. Viadero, Influence of errors in planetary transmissions load sharing under different mesh phasing, Mech. Mach. Theory 153 (2020) 104012.
[44] J. Sánchez-Espiga, A. Fernandez del Rincon, M. Iglesias, F. Viadero, Planetary gear transmissions load sharing measurement from tooth root strains: numerical evaluation of mesh phasing influence, Mech. Mach. Theory 163 (2021) 104370.

[45] J. Sanchez-Espiga, A. Fernandez del Rincon, M. Iglesias, F. Viadero, Use of sun gear orbits to obtain the load sharing in planetary transmissions and its impact in the tooth load, Mech. Mach. Theory 181 (2023) 105216.
[46] G. Huo, M. Iglesias, X. Zhang, et al., Influence of eccentricity error on the orbit of a two-stage double-helical compound planetary gear train with different mesh phasing configurations, Mech. Mach. Theory 196 (2024) 105634.
[47] J.I. Pedrero, M. Pleguezuelos, M. Artés, J.A. Antona, Load distribution model along the line of contact for involute external gears, Mech. Mach. Theory 45 (2010) 780–794.
[48] M.B. Sánchez, M. Pleguezuelos, J.I. Pedrero, Enhanced model of load distribution along the line of contact for non-standard involute external gears, Meccanica 48 (2013) 527–543.
[49] M.B. Sánchez, M. Pleguezuelos, J.I. Pedrero, Approximate equations for the meshing stiffness and the load sharing ratio of spur gears including Hertzian effects, Mech. Mach. Theory 109 (2017) 231–249.
[50] M.B. Sánchez, M. Pleguezuelos, J.I. Pedrero, Calculation of tooth bending strength and surface durability of internal spur gear drives, Mech. Mach. Theory 95 (2016) 102–113.
[51] M.B. Sánchez, M. Pleguezuelos, J.I. Pedrero, Strength model for bending and pitting calculations of internal spur gears, Mech. Mach. Theory 133 (2019) 691–705.
[52] M.B. Sánchez, M. Pleguezuelos, J.I. Pedrero, Influence of profile modifications on meshing stiffness, load sharing, and transmission error of involute spur gears, Mech Mach. Theory 139 (2019) 506–525.
[53] M. Pleguezuelos, M.B. Sánchez, J.I. Pedrero, Analytical model for meshing stiffness, load sharing, and transmission error for spur gears with profile modification under non-nominal load conditions, Appl. Math. Model. 109 (2021) 344–365.
[54] J.I. Pedrero, M.B. Sánchez, M. Pleguezuelos, Analytical model of meshing stiffness, load sharing, and transmission error for internal spur gears with profile modification, Mech Mach. Theory 197 (2024) 105650.
[55] J.I. Pedrero, M. Pleguezuelos, M.B. Sánchez, Influence of meshing stiffness on load distribution between planets of planetary gear drives, Mech. Mach. Theory 170 (2022) 104718.
[56] L. Vedmar, B. Henriksson, A general approach for determining dynamic forces in spur gears, J. Mech. Des. 120 (1998) 593–598.